Colloid Polym Sci 277:719–726 (1999)

ORIGINAL CONTRIBUTION

U. Neuhäusler
S. Abend
C. Jacobsen
G. Lagaly

Soft X-ray spectromicroscopy on solid-stabilized emulsions

Received: 11 December 1998
Accepted in revised form: 10 January 1999

U. Neuhäusler (✉) · C. Jacobsen
Department of Physics and Astronomy
State University of New York
at Stony Brook, Stony Brook
NY 11794-3800, USA
e-mail: uneuhae@xray1.physics.sunysb.edu
Tel.: +1-516-6328097
Fax: +1-516-6328101

U. Neuhäusler
Forschungseinrichtung Röntgenphysik
Georg-August-Universität
D-37073 Göttingen, Germany

S. Abend · G. Lagaly
Institut für Anorganische Chemie
Christian-Albrechts-Universität
D-24098 Kiel, Germany

Abstract Oil–water emulsions stabilized by solids have been imaged with sub-100 nm spatial resolution and analyzed spectroscopically using a scanning transmission X-ray microscope. The emulsions are stabilized by particle heterocoagulate cages surrounding the oil droplets. These cages form due to the interaction of negatively charged clay mineral particles (sodium montmorillonite, Wyoming) and positively charged particles of calcium/aluminum layered double hydroxide (LDH). The emulsions were studied at atmospheric pressure, without any pretreatment using carbon *K* and calcium *L* X-ray absorption edges. Oil- and calcium-rich LDH were separately mapped, and the clay mineral dispersions were also imaged. Applying X-ray absorption-edge contrast, oil could be distinguished from water in the emulsion near the carbon *K* absorption edge (284 eV, 4.4 nm). Spectromicroscopy near the calcium *L* absorption edge (346 eV, 3.6 nm) allowed the structural details of heterocoagulate formation to be revealed.

Key words Layered double hydroxide · Montmorillonite · Pickering emulsions · Soft X-ray spectromicroscopy · Solid-stabilized emulsions

Introduction

Soft X-ray microscopes offer especially favorable contrast mechanisms for studying colloidal systems. Unlike in electron microscopy, samples can easily be examined in transmission in a hydrated state at atmospheric pressure without any pretreatment and with an approximately tenfold higher spatial resolution than achievable in visible light microscopy. The energy range of the so called "water window" [1] between oxygen and the carbon *K* absorption edges (543 eV, 2.3 nm and 284 eV, 4.4 nm) is of particular interest for studies on hydrated samples, for within this energy range water is highly transparent for X rays compared to other substances. In addition, X-ray absorption edges (e.g. for carbon, oxygen, nitrogen, calcium, potassium) can be used to visualize and map compounds containing about 1% more of these elements versus other compounds. We report here on results of using soft X-ray spectromicroscopy to image oil–water emulsions stabilized by solids highlighting different compounds in the sample using X-ray absorption-edge contrast near calcium and carbon absorption edges.

X-ray microscopy

Experimental setup

The X1-A scanning transmission X-ray microscope (STXM)

The X1 undulator at the National Synchrotron Light Source (Figs. 1, 2) is a tunable bright source of soft X-rays for photon energies between 200 and 800 eV and is therefore ideally suited for scanning X-ray microscopy. The X1-A beamline [3] provides a flux of about 10^7 spatially coherent photons per second with an energy bandpass of about 0.1 eV at the carbon *K* edge to the

microscope setup [4, 5]. A Fresnel zone plate (which uses diffractive focusing) was used to form a high-resolution focused spot of soft X-rays. Due to working distance requirements, the zone plate used here has a diameter of 160 μm and an outer most width of 45 nm, with a theoretical Rayleigh resolution of 55 nm [6]. For some experiments reported here, we chose to open illumination apertures in a way that increased the available X-ray flux at the cost of a slight decrease in spatial coherence and thus spatial resolution. The sample is scanned using either stepper motors for coarse, large image fields, or piezoelectric actuators for high-resolution scans of smaller fields. The radiation is detected in transmission by a proportional counter. Spectroscopic information near the X-ray absorption edges can be obtained with the STXM by selecting a small object region of interest and changing the photon energy and the zone plate focus for data aquisition as done for the spectra shown in Fig. 8. The spatial resolution for acquiring such spectra is about 200 nm as limited by imperfections in the way energy-dependent focus corrections are made.

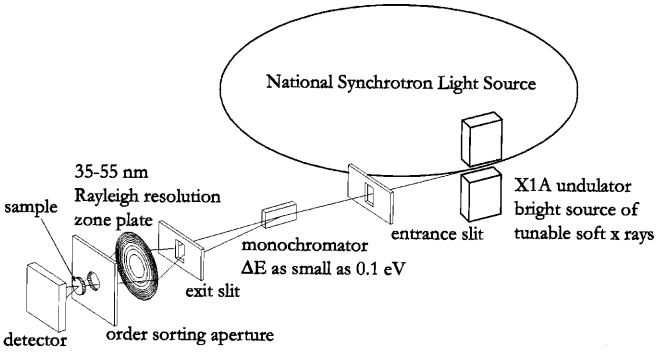

Fig. 1 Simplified schematic of the scanning transmission X-ray microscope (*STXM*) at the X-1A undulator beamline (from Ref. [2]). The actual beamline optics are described by Winn et al. [3]

Wet specimen chamber

The specimen chamber used for the experiments (Fig. 3) allows preparation of a fully hydrated sample as thin layer (thickness approximately 2 μm) between 100 nm-thin silicon nitride windows [7]. The wet cell is sealed by O-rings that prevent the sample from drying out, thereby allowing experiments to be carried out for many hours. Due to the small numerical aperture of zone plate optics currently used, the depth of focus is of the order of micrometers, so the whole sample is within the depth of focus. Since the 1/e attenuation length for water varies between 2 μm at 284 eV and 10 μm at 530 eV, it is important to have hydrated specimens only a few micrometers thick. The design, weight and dimensions of the wet cell are determined by the boundary conditions of the microscope setup.

Theoretical background

Contrast mechanisms

The "water-window" contrast arises from the difference in absorptivity of water and carbonaceous (or other dense inorganic) material (Fig. 4). In addition to the "water-window" contrast for hydrated samples, X-ray absorption-edge contrast can be used to highlight compounds containing a certain element. In a small energy range near the X-ray absorption edges, the transmission properties change rather drastically for the edge element, while the transmission remains almost constant for all other elements; this can be seen in Fig. 4

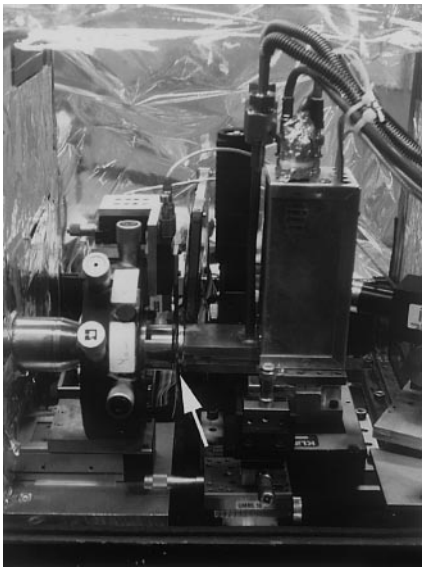

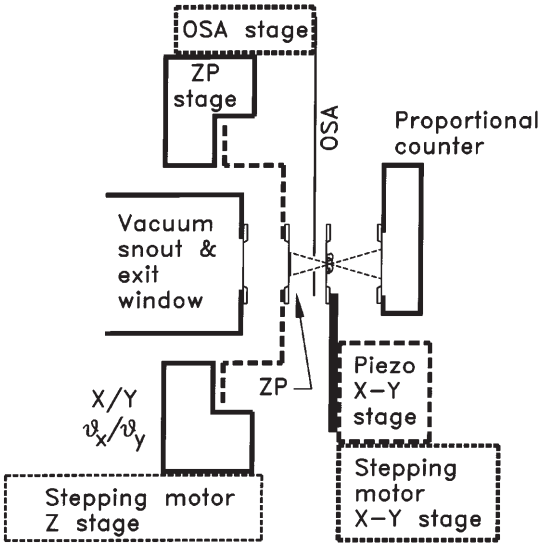

Fig. 2 Photograph and schematic of the Stony Brook STXM at the National Synchrotron Light Source. The zone plate (*ZP*) and specimen chamber are in the region indicated by the *arrow* in the photograph

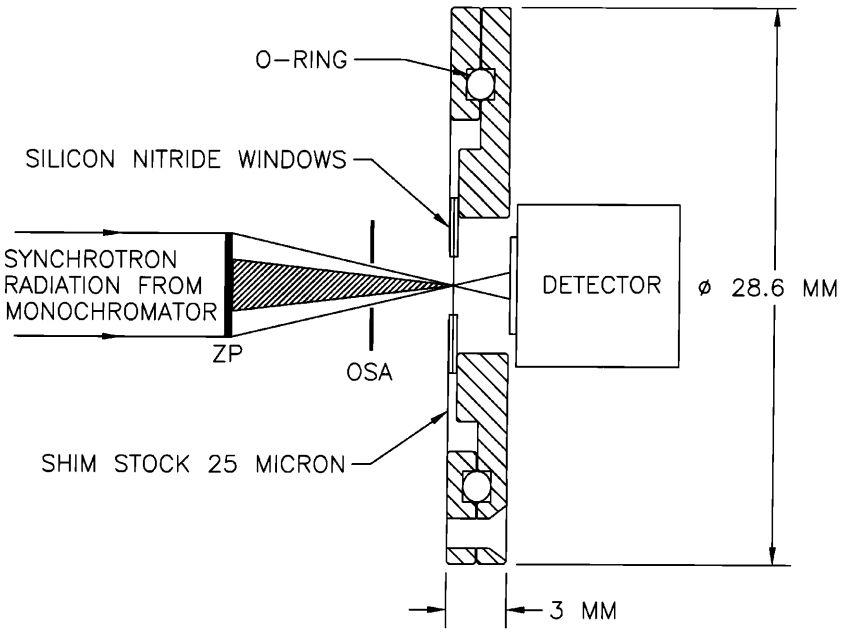

Fig. 3 Cross-section overview of the wet specimen chamber. Note that the 160 μm-diameter ZP and its 70 μm-diameter order-sorting aperture are shown enlarged from their actual size, and the detector is shown reduced from its actual size

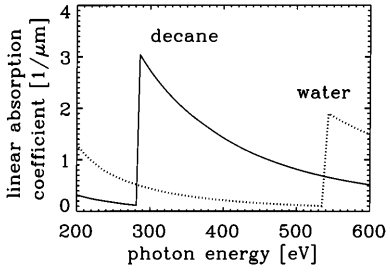

Fig. 4 Linear absorption coefficients for soft X-rays in water and decane, calculated using the optical constants tabulated by Henke et al. [9]. The oxygen and carbon absorption edges are clearly seen in water and decane, respectively. The tabulated absorption data are accurate except for the region within about 10 eV of the absorption edges, where near-edge absorption resonances appear due to electronic transitions to molecular orbitals

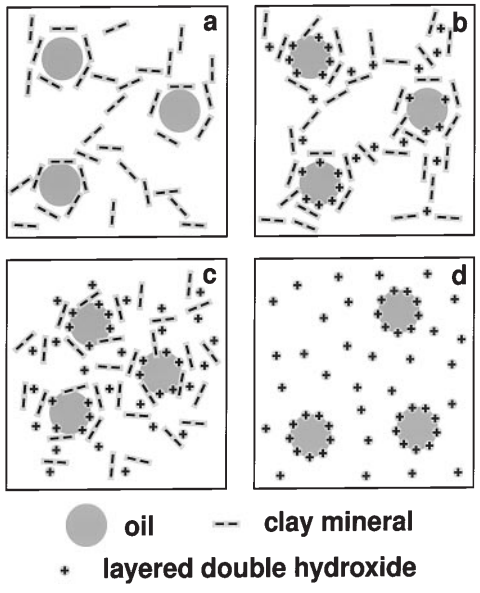

Fig. 5a–d Model of emulsions stabilization by mixtures of montmorillonite and LDH at different mass fractions χ of hydroxide (from Ref. [18]). **a** $\chi = 0$: the oil droplets are enclosed in the network of montmorillonite particles. **b** and **c** heterocoagulation of hydroxide and clay mineral particles: formation of three-dimensional networks which impede coalescence of the oil droplets, **b** $\rightarrow$ **c**: increasing content of hydroxide. **d** $\chi \rightarrow 1$: the oil droplets are stabilized by envelopes of hydroxide particles

which shows absorption spectra of decane and water. The carbon K absorption edge of decane is seen clearly at about 284 eV, and the oxygen K absorption edge for water is at around 543 eV. What is not indicated in Fig. 4 is the presence of X-ray absorption near-edge structure, or XANES resonances. These resonances are the result of electronic transitions from core to outlying states such as unoccupied molecular orbitals. These resonance-like transitions are very sensitive to the kind of chemical bonding and can also be exploited in STXM [8] (Fig. 8).

X-ray optical interactions

The interaction between X-rays and matter in the soft X-ray range is well described by the high-frequency limit of classical anomalous dispersion theory. This theory (see e.g. Refs. [10, 11]) gives a form of the refractive index of

$$n = 1 - \delta - i\beta = 1 - K(f_1 + f_2), \quad (1)$$

where

$$K = \frac{1}{2\pi} r_e \lambda^2 n_a. \quad (2)$$

In the refractive index n, δ is the part representing the phase shift, β describes the absorption, n_a is the number density of atoms, and $r_e = 2.818 \times 10^{-15}$ m is the classical radius of the electron. The energy-dependent refractive index coefficients $(f_1 + if_2)$ have been tabulated by Henke et al. [9] and are available from http://*www-cxro.lbl.gov*. This complex refractive index model of absorption $\exp[-4\pi\beta t/\lambda]$ and phase advance $\exp[i2\pi\delta t/\lambda]$ in material of thickness t provides a complete description of soft X-ray interactions. Because photoelectric absorption dominates over elastic scattering which in turn dominates over inelastic scattering [12], soft X-ray images of thick specimens are free of any "haze" caused by multiple scattering. In the refractive-index model, and X-ray beam of incident intensity I_0 which passes through a material of thickness t is attenuated to an intensity I as described by the Lambert–Beer law:

$$I = I_0 \exp(-\mu t), \quad (3)$$

where $\mu = 4\pi\beta/\lambda$ is the linear absorption coefficient in units of 1/length (see Fig. 4). In experiments, the sample thickness is often not well defined. Equation (4) allows one to characterize a sample in terms of its mass per area $d = \rho t$ if its thickness is not otherwise known, and this analysis method is followed here:

$$I = I_0 \exp(-\mu t) = I_0 \exp\left(-\frac{\mu}{\rho}\rho t\right) = I_0 \exp\left(-\frac{\mu}{\rho} d\right). \quad (4)$$

Note, that the element's density ρ is needed to write the dependencies in a way suited for further evaluation, but the density does not need to be known explicitly. Using Eqs. (1) and (2), μ/ρ can be calculated as

$$\frac{\mu}{\rho} = 2\frac{N_A}{M} r_e \lambda f_2(\lambda) = 3.394 \times 10^{11}\ \text{cm} \quad \frac{f_2(\lambda)}{M}\lambda, \quad (5)$$

where N_A is Avogadro's number and M is the molar mass, and compounds and molecules can be modeled by calculating (f_2/M) as a weighted sum over all elements.

Quantitative elemental mapping near X-ray absorption edges

Away from an element's absorption edge, its linear absorption coefficient varies as $\mu \propto \lambda^3$ and so a 1% change in wavelength produces only a 3% change in absorption. On the other hand, at absorption edges the linear absorption coefficient μ can change by a factor of 10 or more with an energy change of less than 1%, as illustrated in Fig. 4. This allows one to quantitatively map the concentration of an element by taking two images on either side of its X-ray absorption edge, provided the element is present at a concentration of about 1% or more.

To determine the mass per area $d_y = \rho_y t_y$ of a specific element y among the mass per area $d_r = \rho_r t_r$ of the remaining elements, one can use images at wavelengths λ_1 and λ_2 on the strongly absorbing λ_1 and weakly absorbing λ_2 sides of the element's absorption edge. The intensity of each image is then given by

$$I_{11} = I_{01} \exp\left(-\left(\frac{\mu_1}{\rho}\right)_y d_y - \left(\frac{\mu_1}{\rho}\right)_r d_r\right) \quad (6)$$

and

$$I_{12} = I_{02} \exp\left(-\left(\frac{\mu_2}{\rho}\right)_y d_y - \left(\frac{\mu_2}{\rho}\right)_r d_r\right), \quad (7)$$

where I_{11}/I_{12} are transmitted intensities at the high/low-energy side of the edge. If we assume that the other elements with mass density $d_r = \rho_r t_r$ have an absorption coefficient that varies as λ^3, we can eliminate $d_r = \rho_r t_r$ and solve for the mass per area of element y using an expression first obtained by Engström [13]:

$$d_y = \rho_y t_y = \frac{\ln\left(\frac{I_{01}}{I_{11}}\right) - \left(\frac{\lambda_1}{\lambda_2}\right)^3 \ln\left(\frac{I_{02}}{I_{12}}\right)}{\left(\frac{\mu_1}{\rho}\right)_y - \left(\frac{\mu_2}{\rho}\right)_y \left(\frac{\lambda_1}{\lambda_2}\right)^3}, \quad (8)$$

where $(\mu_i/\rho)_y$ can be calculated from the Henke data following Eq. (5). For demonstrating the method of quantitative analysis, this approach is sufficient. More detailed calculations can use measured or tabulated values for $d_r = \rho_r t_r$ rather than assume as λ^3 scaling; such calculations have been used by Buckley [14] for the quantitative mapping of calcium in bone.

The above analysis allows us to quantify the mass per area of calcium in images of aqueous calcium/aluminum layered double hydroxide (LDH) suspensions and in emulsions using calcium/aluminum LDH as an emulsifying agent. To do so, the absorption spectrum of a hydrated layer of pure calcium/aluminum LDH was measured separately (Fig. 8a). This spectrum shows that the calcium L edge has two strong near-edge absorption resonances [15] which enhance the sensitivity of calcium maps. For absolute calibration using the tabulated absorption coefficient f_2, a step-edge was fitted to the pre- and post-edge regions of the absorption spectrum as described by Buckley [14]. Buckley has also shown that low-mass-per-area calcium can be mapped with a high degree of accuracy by this means provided a high-resolution monochromator is used [16]. These conditions have been met in our experiments. To quantify calcium, we took images at a pre-edge energy (346 eV) and a XANES resonance energy (352 eV) (Figs. 6, 10), and used the step-edge normalized calcium spectrum of Fig. 8a for calcium quantification.

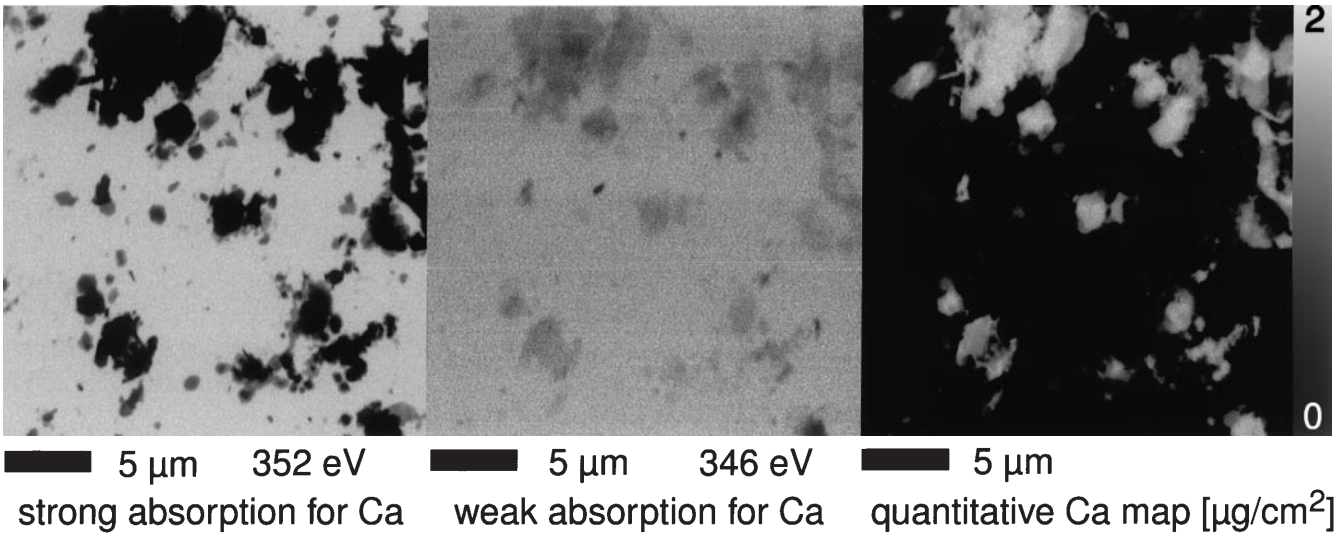

Fig. 6 STXM images of an aqueous dispersion containing 0.5% (w/w) calcium/aluminum LDH taken at the photon energies indicated in Fig. 8a near the calcium absorption edge. The calcium map (*right image*) is calculated from the *left* and *center images* (strong and weak absorption for calcium); the *gray scale bar* indicates the amount of calcium. The images have 300 × 300 pixels with a pixel size of 80 nm

Oil–water emulsions stabilized by solids

Motivation

It has been known for a long time that colloidal particles can act as stabilizers in emulsions [17]. The surface of the clay mineral usually has to be modified by organic cations in order to obtain a stable emulsion. The oil-water emulsions examined here have been stabilized only by a clay mineral (sodium montmorillonite, Wyoming) and calcium/aluminum LDH without any additional surface-active agents [18]. The idea behind this was that pronounced stabilization will be attained when two types of particles with different charges are used: clay minerals with negatively charged layers and LDH with positively charged layers. The interaction between the clay mineral and the LDH particles leads to the formation of heterocoagulates. These heterocoagulates surround and cage the oil droplets in the emulsion and prevent them from coalescing and forming a separate oil/water phase (Fig. 9). This new technique of stabilizing emulsions is of interest for a large variety of applications in cosmetics and pharmaceutical products, because it is desirable to avoid surfactants from a environmental and toxicological point of view.

Materials

The process of making these solid stabilized oil–water emulsion, and measurements on their rheology and coalescence properties are described elswhere [18]. We concentrate here on the X-ray microscopy experiments.

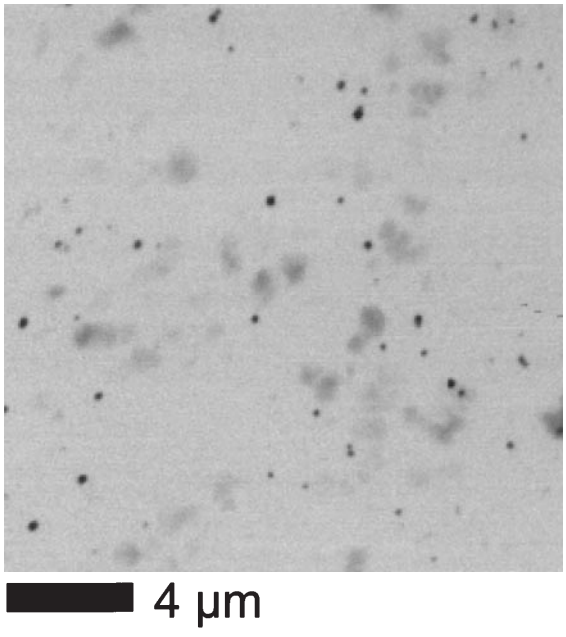

Fig. 7 STXM image of an 1% (w/w) aqueous sodium montmorillonite dispersion, taken at a photon energy of 290 eV (250 × 250 pixels, 70 nm pixel size)

The emulsions analyzed with STXM contained water, 10% (v/v) paraffin oil, and a total amount of 1% (w/w) solid in different ratios of clay mineral and LDH. For the preparation in the wet cell, the emulsions were diluted with water to 0.1% (w/w) solid content and 1% (v/v) oil. Two emulsions are shown one with the same amount of montmorillonite and LDH ($\chi = 0.5$), the other ($\chi = 1$) only containing LDH as the emulsifying agent.

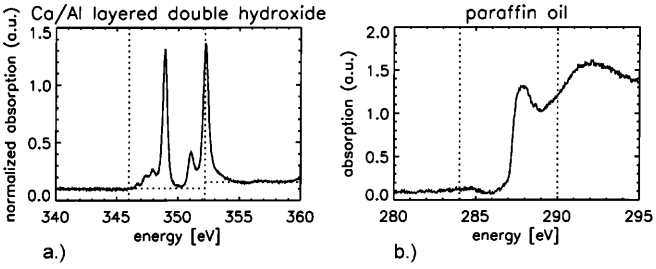

Fig. 8a, b Near edge absorption spectra taken in the STXM. **a** X-ray absorption spectrum of calcium/aluminum layered double hydroxide (*LDH*) dispersed in water near the calcium *L* absorption edge. The spectrum is normalized in order to quantitatively determine the height of the absorption-edge step as indicated by the *horizontal dashed lines*. **b** X-ray absorption spectrum of paraffin oil (bulk sample) near the carbon *K* absorption edge. For both plots, the photon energies used for taking the images shown in Fig. 9 and 10 are marked with *vertical dashed lines*

Results

Our goal was to better understand the stabilizing process in these emulsions using the X-ray microscope for high-resolution imaging and spectromicroscopic mapping of calcium and carbon.

Single compounds

To be able to compare the aggregation of the clay mineral and LDH in the emulsions to that of the single components, montmorillonite and LDH particles were imaged separately (Figs. 6, 7). Aqueous montmorillonite has already been studied in a transmission X-ray microscope (TXM) [19]. The contrast for the clay mineral in the image shown in Fig. 7 is very weak due to the fact that the sodium montmorillonite is completely delaminated. As a result, the clay mineral does not appear in the form of aggregates, but as small primary particles. The black spherical particles in the image appear to be quartz.

XANES spectroscopy

In order to find photon energies suited for absorption-edge contrast imaging, the absorptivity of oil/LDH was characterized first by taking absorption spectra near the carbon and calcium absorption edges (Fig. 8). Photon energies chosen for imaging are marked with dashed lines. The absorption peak for paraffin oil at around 287.5 eV is rather wide due to the overlap of many resonances caused by transitions from many different bonding states. For the spectra of the LDH near the calcium edge, the absorption peaks corresponding to the L_{II}/L_{III} shell electron transitions are shifted by 3 eV to higher energies compared to tabulated values [9] due to the ionic state of calcium in the sample.

Differential imaging near absorption edges

In a single image at one photon energy, it is not possible to unambiguously identify oil droplets versus clay mineral, quartz particles or LDH concentrations. Therefore, differential imaging at different photon energies was applied both near carbon and calcium X-ray absorption edges. Taking advantage of absorption-edge contrast for emulsion $\chi = 0.5$, oil could be distinguished from water near the carbon *K* edge. Near the calcium *L* edge, the calcium/aluminum LDH could be highlighted and thus distinguished from the clay mineral (contains no calcium) by taking images at photon energies with characteristic absorption properties for calcium (Fig. 9a,b).

A contrast reversal between water and oil can be observed when comparing images in Fig. 9c,d and d. This is in agreement with the absorption coefficients as calculated and shown in Fig. 4, where we used decane to approximate the absorption of the more complex makeup of paraffin oil.

For the image in Fig. 9a, the calcium-rich LDH is transparent and only the clay mineral aggregates are visible. They look more dense than in the pure montmorillonite dispersion (Fig. 7) because of aggregation caused by calcium and aluminum ions of the LDH and formation of the heterocoagulate.

Figure 10 shows a Pickering emulsion ($\chi = 1$), that is stabilized only by one solid compound, namely LDH. At a photon energy where calcium is strongly absorbing, it is not possible to decide if this is only a LDH aggregate or a stabilized oil droplet. The image taken for high-calcium transmission reveals the oil droplet inside the LDH envelope.

For the emulsion $\chi = 1$, the colloidal particles are located right in the interface of oil and water (Fig. 10) as predicted for Pickering emulsions, while the heterocoagulate structures at $\chi = 0.5$ extend rather far away from the oil/water interface (Fig. 9).

Outlook

The emulsions studied here have also been examined in a TXM [20]. The TXM is advantageous for quick imaging at a fixed photon energy with high spatial resolution; however, the spectral information obtained with STXM is currently not accessible in a TXM [21].

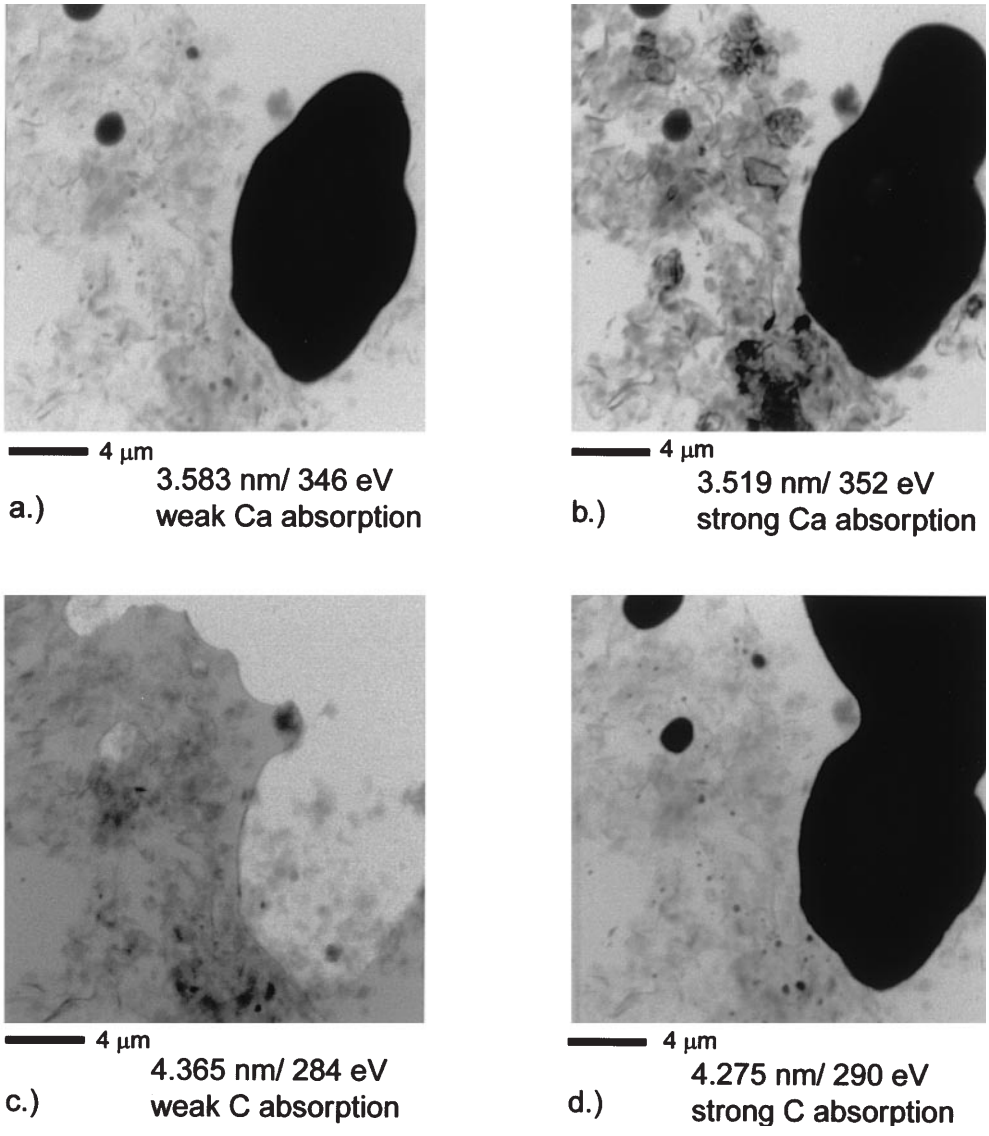

Fig. 9a–d Images of the emulsion $\chi = 0.5$, which contains equal amounts of montmorillonite and LDH near calcium and carbon X-ray absorption edges. The photon energies used are indicated in Fig. 8. **a** Calcium weakly absorbing, the clay mineral is visible. **b** Calcium strongly absorbing, LDH is visible. **c** Carbon weakly absorbing, the paraffin oil droplet is transparent. **d** Carbon strongly absorbing, the oil droplet appears black. The images were taken over a time period 2 h in the sequence **a**, **b**, **d**, **c**. During the experiment, the oil droplet caged by heterocoagulates remained at a fixed position (*lower part* of the image), while the part of the oil droplet in a region without a stabilizing envelope (*at top*) began to disperse. The images have 300×300 pixels with a pixel of 70 nm. The data acquisition time was 10(20) min for images taken near the calcium (carbon) edge

Cryo techniques have been applied to X-ray microscopy in a TXM [22] as well as in a STXM [23]. This is of particular interest for biological samples, where the high radiation dose required to obtain high-quality images with high spatial resolution (up to 10^7 Gy) induces visible structural changes in the sample. However, the radiation sensitivity strongly depends on the kind of material examined. We have no evidence that the samples described here suffer radiation damage that changes their properties during the experiment. In addition, the radiation dose delivered to the specimen is lower in STXM, where the specimen is followed by an X-ray detector, than in TXM, where a 10–20% efficient zone plate and a detector follow the specimen.

Conclusion

It has been shown that STXM is capable of analyzing in situ emulsions with both high spectral (~0.1 eV) and spatial (under ideal conditions 55 nm) resolution, and is therefore capable of distinguishing between their four single compounds, oil, water clay mineral (sodium montmorillonite) and calcium/aluminum LDH. X-ray absorption edges made it possible to map the elements carbon and calcium in the sample and, therefore, to distinguish. This is based on the natural absorptivity properties of the sample and does not require any sample treatment. Calculations on the X-ray optical properties of the sample in combination

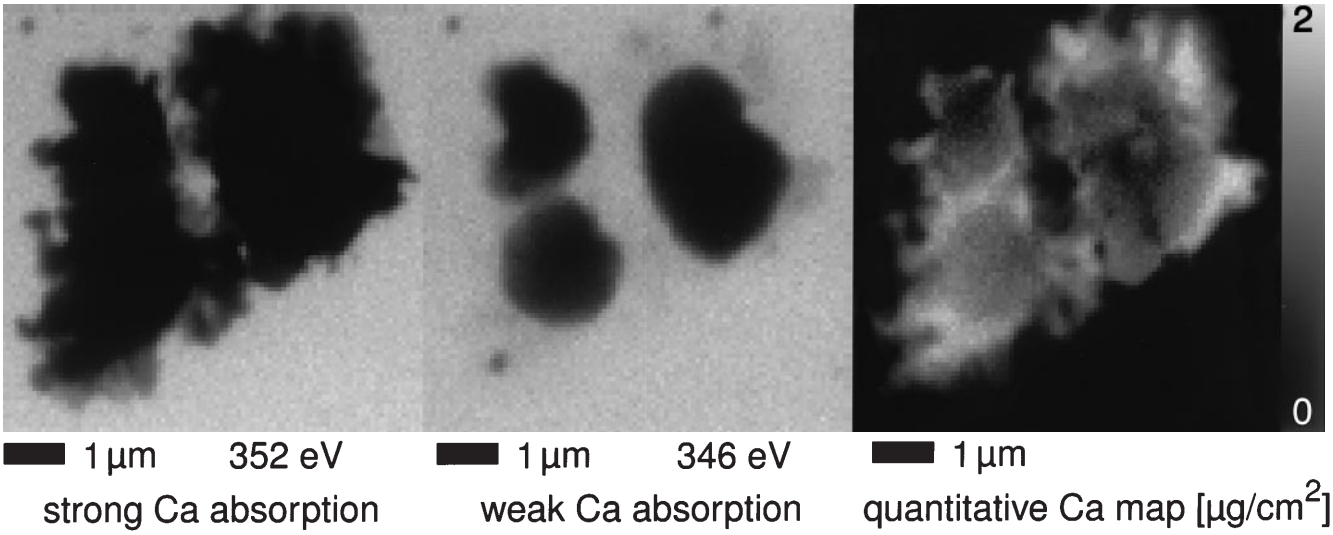

Fig. 10 STXM images of the Pickering emulsion $\chi = 1$ (which contains only LDH as a solid compound), taken near the calcium *L* edge. From left to right: strong/weak absorption for calcium, quantitative calcium map (the *gray scale bar* indicates the amount of calcium). The image has 96×96 pixels with a pixel size of 75 nm

with experimental calcium XANES spectroscopy data of the calcium/aluminum LDH were used to quantitatively map the calcium concentration in the sample. To our knowledge, the information obtained with this technique is currently not accessible by any other means.

Acknowledgements This work was supported by a fellowship (U.N.) for Ph.D. research studies (Doktorandenstipendium HSP III) from the German Academic Exchange Service (DAAD), by the Office of Biological and Environmental Research, US DoE under contract DE-FG02-89ER60858, and by a travel grant (S.A.) from the Boehringer Ingelheim Fonds for basic medical research. We would like to thank our collegues at Stony Brook and in particular Sue Wirick for her help at the beamline.

References

1. (a) Wolter H (1952) Ann Phys 10: 94; (b) Wolter H (1952) Ann Phys 10:286
2. Wang Y (1998) PhD thesis, State University of New York at Stony Brook, New York
3. Winn B, Ade H, Buckley C, Howells M, Hulbert S, Jacobsen C, Kirz J, McNulty I, Miao J, Oversluizen T, Pogorelsky I, Wirick S (1996) Rev Sci Instrum 67:1
4. Jacobsen C, Williams S, Anderson E, Browne MT, Buckley CJ, Kern D, Kirz J, Rivers M, Zhang X (1991) Opt Commun 86:351
5. Jacobsen C, Anderson E, Chapman H, Kirz J, Lindaas S, Rivers M, Wang S, Williams S, Wirick S, Zhang W (1993) In: Aristov VV, Erko AI (eds) Proceedings of the 4th International Conference X-ray microscopy IV, Bogorodskii Pechatnik Publishing Company, Chernogolovka, Moscow, Russia, pp 304–321
6. Spector S, Jacobsen C, Tennant D (1998) In: Thieme J, Schmahl G, Umbach E, Rudolph D (eds), X-ray microscopy and spectromicroscopy. Springer, Berlin Heidelberg New York, p IV-13
7. Neuhäusler U, Jacobsen C, Schulze D, Stott D, Abend S (1999) J Synchrotron Radiat (accepted)
8. Ade H, Zhang X, Cameron S, Costello C, Kirz J, Williams S (1992) Science 258:972
9. Henke BL, Gullikson EM, Davis JC (1993) At Data Nuc Data Tables 54:181
10. James RW (1982) The optical principles of the diffraction of X-rays. Ox Bow Press, Woodbridge, Connecticut
11. Henke BL (1981) In: Attwood DT, Henke BL (eds) Low energy X-ray diagnostics; vol 75. American Institute of Physics, Monterey, pp 146–155
12. Hubbel JH, Gimm HA, Øverbø I (1980) J Phys Chem Ref Data 9: 1023
13. Engström A (ed) (1962) X-ray microanalysis in biology and medicine. Elsevier, Amsterdam
14. Buckley CJ (1995) Rev Sci Instrum 66:1318
15. Connerade JP (1978) Contemp Phys 19:415
16. Buckley CJ, Bellamy SJ, Zhang X, Dermody G, Hulbert S (1995) Rev Sci Instrum 66:1322
17. Pickering SU (1907) J Chem Soc 97:2001
18. Abend S, Bonnke N, Gutschner U, Lagaly G (1998) Colloid Polym Sci 276:730
19. Niemeyer J, Thieme J, Guttman P, Wilhein T, Rudolph D, Schmahl G (1994) Prog Colloid Polym Sci 95:139
20. Thieme J, Abend S, Lagaly G (1999) Colloid Polym Sci (in press)
21. Neuhäusler U (1996) Diplomarbeit. Universität Göttingen, Göttingen
22. Schneider G, Niemann B (1998). In: Thieme J, Schmahl G, Umbach E, Rudolph D (eds) X-ray microscopy and spectromicroscopy. Springer, Berlin Heidelberg New York, p I-15
23. Maser J, Jacobsen C, Osanna A, Wang S, Kalinovsky A, Kirz J, Spector S, Warnking J (1998) In: Thieme J, Schmahl G, Umbach E, Rudolph D (eds) X-ray microscopy and spectromicroscopy. Springer, Berlin Heidelberg New York, p I-35